Hough Transform and 3D SURF for Robust Three Dimensional Classification

Jan Knopp[1], Mukta Prasad[2], Geert Willems[1],
Radu Timofte[1], and Luc Van Gool[1,2]

[1] KU Leuven
[2] ETH Zurich

Abstract. Most methods for the recognition of shape classes from 3D datasets focus on classifying clean, often manually generated models. However, 3D shapes obtained through acquisition techniques such as Structure-from-Motion or LIDAR scanning are noisy, clutter and holes. In that case global shape features—still dominating the 3D shape class recognition literature—are less appropriate. Inspired by 2D methods, recently researchers have started to work with local features. In keeping with this strand, we propose a new robust 3D shape classification method. It contains two main contributions. First, we extend a robust 2D feature descriptor, SURF, to be used in the context of 3D shapes. Second, we show how 3D shape class recognition can be improved by probabilistic Hough transform based methods, already popular in 2D. Through our experiments on partial shape retrieval, we show the power of the proposed 3D features. Their combination with the Hough transform yields superior results for class recognition on standard datasets. The potential for the applicability of such a method in classifying 3D obtained from Structure-from-Motion methods is promising, as we show in some initial experiments.

1 Introduction

A number of methods for 3D shape class recognition have been proposed already. So far, the dominant line of work has been to use global features, *i.e.* features that need the complete, isolated shape for their extraction. Examples are Fourier or spherical harmonics [1,2], shape moments [2], shape histograms [3]. There are at
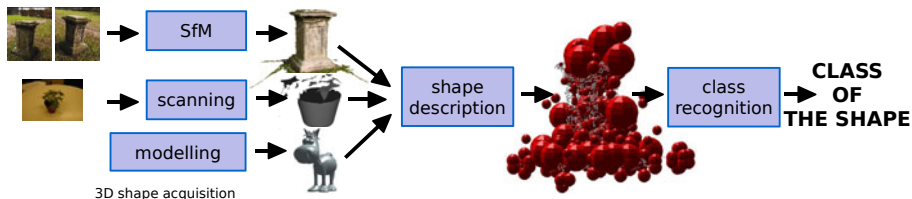

Fig. 1. Proposed approach classifies noisy 3D shapes obtained from SfM, scans etc. The method is invariant to the texture and recognizes difficult objects such as plants.

least three potential problems with these global approaches: (i) it is difficult to handle partial shapes. For instance, when an artifact has been damaged, even the most perfect scan will still only capture a part of what the original shape should have been, (ii) many capturing scenarios contain irrelevant, neighbouring clutter in addition to the relevant data coming from the object. Global methods mix the two, jeopardizing class recognition. Some local, skeleton-based descriptions are also known to suffer from these problems (e.g. [4]), (iii) several classes contain deformable shapes, some parts of which may be more deformable than other more rigid parts. Global methods are also less successful at handling intra-class variations while remaining sufficiently discriminative to noise, clutter, articulated deformations and inter-class variations. In many 3D application based on retrieval, classification and detection, all these three problems have to be addressed.

As work in 2D object class recognition has shown, the use of local rather than global features is advantageous. 2D class detection methods deal with occlusions and clutter quite successfully already. We therefore seek to apply these techniques to the 3D case as well. So far, relatively few 3D categorisation methods based on local features, like tensors [5], heat kernel signatures [6], integral shape descriptors [7,8], and scale dependent features [9] have been proposed.

Ovsjanikov *et al.* [10] extended the standard bag-of-features (BOF) approach of Sivic and Zisserman [19] by looking for the frequency of word pairs instead of the single word, called spatially-sensitive bags of features. Toldo *et al.* [11] described 3D shapes by splitting them into segments, which are then described on the basis of their curvature characteristics. These descriptors are quantized into a visual vocabulary. Finally, an SVM is learnt for the actual categorisation. Methods that use other information than pure shape (e.g. [12,13]) are not considered here because we are interested in the still-common case where no other information is available.

The afore-mentioned methods assume clean, pre-segmented shapes, *i.e.* without them being attached to a 3D 'background'. As such, these BOF approaches could suffer from the problem that the information can get buried under clutter, especially when the object of interest is small compared to this background. In 3D this difference is magnified. For instance, a statue of a person in front of a building may cover a large part of the 2D image scene, but will be tiny compared to the size of the building in 3D, where all objects appear with their actual, relative scales. In Hough transform based approaches, the process of recognition is tied up with hypothesis verification (through object localization). This means that it has higher discriminative power against clutter than BOF based approaches.

This paper proposes an approach to 3D shape categorisation that can perform better at the tasks described above. A 3D extension to SURF [14] serves as our local descriptor described in § 2. This feature has proved quite effective in 2D and can now be viably computed even in 3D. In contrast to a dense or random coverage with spin images [15], a 3D interest point detector picks out a repeatable and salient set of interest points. These descriptors are quantized and used in a Hough approach, like Implicit Shape Model (ISM) [16], which keeps
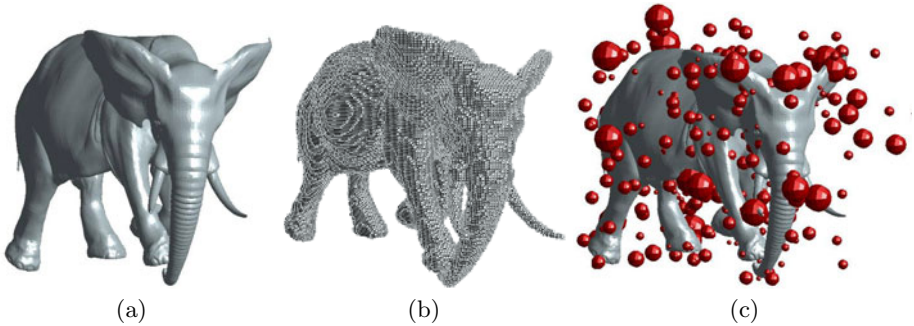
Fig. 2. Illustration of the detection of 3D SURF features. The shape (a) is voxelized into the cube grid (side of length 256) (b). 3D SURF features are detected and back-projected to the shape (c), where detected features are represented as spheres and with the radius illustrating the feature scale.

the influence of each feature better localized than in a BOF approach as seen in § 3. Our approach favorably compares to the state-of-the-art in 3D shape class recognition and retrieval as seen in § 4, § 5.

2   Shape Representation as the Set of 3D SURF Features

For our problem of class recognition, we collected a set $\mathcal{M}$ of shapes separated into two disjoint sets: (i) training data $\mathcal{M}_T$ and (ii) query data $\mathcal{M}_Q$. The mth 3D shape is represented as $\{\mathtt{V_m}, \mathtt{F_m}\}$, where $\mathtt{V_m}$ is a collection of vertices and $\mathtt{F_m}$ is a collection of polygons (specifically triangles) defined on these vertices.

In order to describe each shape $m \in \mathcal{M}$ as a set of local rotation and scale-invariant interest points, we propose an extension of SURF to 3 dimensions. It is important to note at this point, that this extension can also be seen as a special case of the recently proposed Hessian-based spatio-temporal features by Willems *et al.* [17], where temporal and spatial scale are identical. As such, the theoretical results that were obtained from scale space theory still hold. Furthermore, most of the implementation details can be reused, except the fact that the search space has now shrunk from 5 to 4 dimensions (x, y, z, σ). For more in-depth information on Hessian-based localization and scale selection in 3 dimensions, we refer the reader to [17].

The extraction of the 3D features is as follows. First, we voxelize a shape in a volumetric 3D cube of size 256^3 using the intersection of faces with the grid-bins as shown in figure 2(b), after each shape is uniformly scaled to fit the cube while accounting for a boundary of 40 at each side. The cube parameters were chosen empirically. Next, we compute a saliency measure S for each grid-bin $\boldsymbol{x}$ and several scales σ (over three octaves). We define S as the absolute value of the determinant of the Hessian matrix $H(\boldsymbol{x}, \sigma)$ of Gaussian second-order derivatives $L(\boldsymbol{x}, \sigma)$ computed by box filters,

$$S(\boldsymbol{x}, \sigma) = \big|H(\boldsymbol{x}, \sigma)\big| = \left| \begin{pmatrix} L_{xx}(\boldsymbol{x}, \sigma) \; L_{xy}(\boldsymbol{x}, \sigma) \; L_{xz}(\boldsymbol{x}, \sigma) \\ L_{yx}(\boldsymbol{x}, \sigma) \; L_{yy}(\boldsymbol{x}, \sigma) \; L_{yz}(\boldsymbol{x}, \sigma) \\ L_{zx}(\boldsymbol{x}, \sigma) \; L_{zy}(\boldsymbol{x}, \sigma) \; L_{zz}(\boldsymbol{x}, \sigma) \end{pmatrix} \right|, \tag{1}$$

as proposed in [17]. This has as implication that, unlike in the case of SURF [14], a positive value of S does not guarantee that all eigenvalues of H have identical signs. Consequently, not only blob-like signals are detected, but also saddle points. Finally, K_m unique features: $\mathbf{d}_{mk}, k \in \{1 \ldots K_m\}$ are extracted from the volume using non-maximal suppression (see [17] for more details).

In a second stage, a rotation and scale-invariant 3D SURF descriptor is computed around each interest point. First, we compute the local frame of the feature. We therefore uniformly sample Haar-wavelet responses along all 3 axes within a distance $3 \times \sigma$ from each feature. Next, each response is weighted with a Gaussian centered at the interest point, in order to increase robustness to small changes in position. Each weighted response is plotted in the space spanned by the 3 axes. We sum the response vectors in all possible cones with an opening angle of $\pi/3$ and define the direction of the longest resulting vector as the dominant orientation. However, instead of exhaustively testing a large set of cones uniformly sampled over a sphere, we approximate this step by putting a cone around each response. After the dominant direction has been obtained, all responses are projected along this direction after which the second orientation is found using a sliding window [14]. The two obtained directions fully define the local frame. Defining a $N \times N \times N$ grid around the feature and computing the actual descriptor, is implemented as a straight-forward extension of the 2D version. At each grid cell, we store a 6-dimensional description vector of Haar wavelet responses as in [17]. In the rest of the paper, we assume $N = 3$.

For the feature k of the shape m we maintain a tuple of associated information as shown below:

$$\mathbf{d}_{mk} = \Big\{ \underset{3 \times 1}{\mathbf{p}_{mk}} \;\;, \;\; \sigma_{mk} \;\;, \;\; \underset{162 \times 1}{\mathbf{s}_{mk}} \Big\}, \tag{2}$$

where $\mathbf{p}_{mk}$ represents the relative 3D position of the feature point to the shape's centre, σ_{mk} is the scale of the feature point and $\mathbf{s}_{mk}$ is 162-dimensional 3D SURF descriptor vector[1] of the feature vector $\mathbf{d}_{mk}$.

3   Implicit Shape Model for 3D Classification

In order to correctly classify query shapes, we need to assemble a model of each class based on the local 3D SURF features, and define a ranking function to relate a shape to each class. The Implicit Shape Model converts the SURF features to a more restricted 'visual vocabulary' generated from training data. We will discuss this in § 3.1. Based on the information acquired during training, each visual word on a query shape then casts weighted votes for the location of the shape center for a particular class, which will be seen in § 3.2. Depending

---

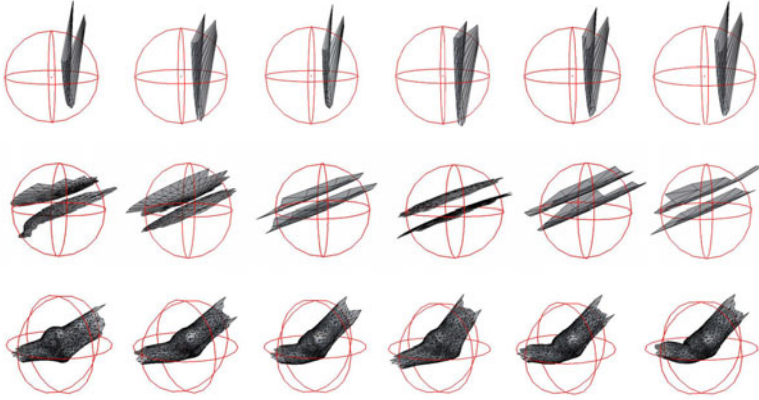[1] $3 \times 3 \times 3 \times 6 = 162$.

Fig. 3. Each row shows some partial 3D shapes from which features were computed that belong to the same visual word. The feature center is represented as a red dot, while the sphere represents the feature scale. Each shape is shown normalized with respect to the scale of the feature.

on whether the query shape's center is already known, the above information is used for classification in two ways as outlined in § 3.3.

3.1   Visual Vocabulary Construction

To reduce the dimensionality of feature matching and limit the effects of noise, we quantize the SURF features to a vocabulary of visual words, which we define as the cluster centers of an approximate K-means algorithm (see Muja *et al.* [18]). Following standard practice [19,20] in large-scale image searching, we set the number of visual words (clusters) to 10% of the total number of features in our training set. In practice, this yields a reasonable balance between mapping similar shapes to the same visual word (Fig. 3) while ensuring that features that are assigned the same word are indeed likely to correspond (Fig. 4).

3.2   Learning and Weighting Votes

Rather than storing a shape for each class, the ISM-based methods keep track of where a visual word v would be located on a shape of class c relative to c's center ([16,21]). This information — the collection of visual words and offsets from shape centers — is assembled from the training set, and stored along with the visual words themselves. Word v is therefore associated with a list of votes, each of those being generated from a feature (introduced in Eq. 2) and defined by the feature's class c, its vector to the shape center (x', y', z'), its scale σ', and the scale of the shape. Each word may therefore cast votes for multiple classes. Words may also cast multiple votes for the *same* class, as in Fig. 5, because there may be multiple features on a shape associated with the same visual word.

Suppose now that a query shape contains a feature at location $[x, y, z]^T$ with scale σ that is assigned to visual word v. That feature will cast a vote, λ, for a shape of class c centered at location
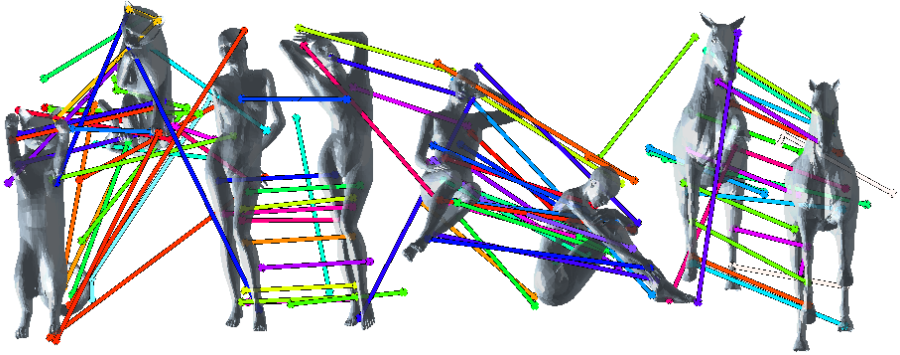
Fig. 4. Examples of visual vocabulary based correspondences between 3D shapes

$$\lambda = \left[x - x'(\sigma/\ \sigma'), y - y'(\sigma/\ \sigma'), z - z'(\sigma/\ \sigma'), \sigma/\ \sigma' \right]^T, \tag{3}$$

with relative shape size $\sigma/\ \sigma'$. If the query shape exactly matches a training shape, the votes associated with that training shape will all be cast at the query shape's center, making a strong cluster of votes for the match. On the other hand, the votes associated with a training shape from a different class will get scattered around, because the spatial arrangement of features (and therefore visual words) will be different, see Fig. 5.

Note that although a single assignment of features to the closest visual word is natural, it is subject to noise when cluster centers are close together. Therefore, during the training phase, each feature activates the closest word and every other word within a distance τ, as in [16,20,22]. This ensures that similar visual words that are located at the same position on a shape will all vote appropriately.

An issue is that different classes may have different numbers of features, and not all features discriminate equally well between classes. We account for these next discuss factors with a pair of weights,

(i) a statistical weight W_{st} as every vote should be invariant to the number of training samples in the class,
(ii) a learned weight W_{lrn} weights every vote so it correctly votes for a class centre across training shapes.

(i) The statistical weight $W_{st}(c_i, v_j)$ weights all the votes cast by visual word v_j for class c_i by

$$W_{st}(c_i, v_j) = \frac{1}{n_{vw}(c_i)} \cdot \frac{1}{n_{vot}(v_j)} \cdot \frac{\frac{n_{vot}(c_i, v_j)}{n_{ftr}(c_i)}}{\sum_{c_k \in \mathcal{C}} \frac{n_{vot}(c_k, v_j)}{n_{ftr}(c_k)}}, \tag{4}$$

where the different numbers n are determined from the training set. For instance, $n_{vot}(v_j)$ is the total number of votes from visual word v_j, $n_{vot}(c_i, v_j)$ is the
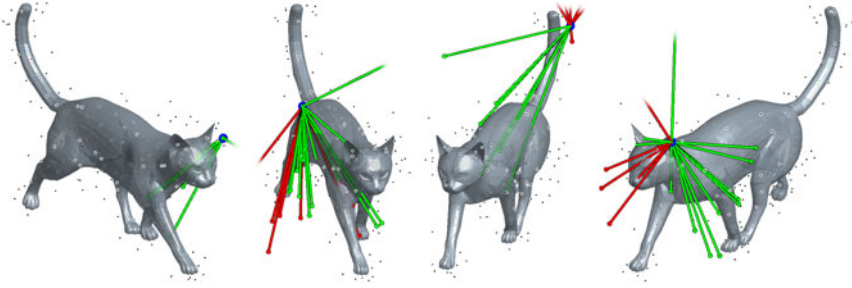
Fig. 5. Example of the votes cast from four features on a cat shape instance. All detected features are visualized as small black dots and votes are shown as lines starting from the feature (marked blue). The votes from a toy ISM model were learned from six shapes of the cat-class (visualized as green lines) and six shapes of flamingo-class (red lines).

number of votes for class c_i from v_j, $n_{vw}(c_i)$ is the number of visual words that vote for class c_i, $n_{ftr}(c_i)$ is the number of features from which c_i was learned. $\mathcal{C}$ is the set of all classes. The first term makes every class invariant to the number of visual words in its training set, while the second normalizes for the number of votes each visual word casts. The final term reflects the probability that v_j votes for class c_i as opposed to some other class.

(ii) Additionally, motivated by Maji's *et al.* [23] work, we normalize votes on the basis of how often they vote for the correct training shape centers (during training). We define λ_{ij} as the vote cast by a particular instance of visual word v_j on a particular *training* shape of class c_i; that is, λ_{ij} records the distance of the particular instance of visual word v_j to the center of the training shape on which it was found. We now apply this vote to *every* instance of visual word v_j on *every* training shape in class c_i, and compute a Gaussian function of the distance between the center position voted for and the actual center. This scheme puts more emphasis on features with voted positions close to that actual center.

For every vote λ_{ij}, our goal is to obtain one value summarizing the statistics of distances to shape centers,

$$W_{lrn}(\lambda_{ij}) = f\left(\left\{ e^{-\frac{d_a(\lambda_{ij})^2}{\sigma^2}} \;\middle|\; a \in A \right\}\right), \tag{5}$$

where A is the set of all features associated with word v_j on a shape of class c_i and $d_a(\lambda_{ij})$ is the Euclidean distance as just defined. We use a standard deviation of σ taken as 10% of the shape size, which defines the accepted amount of noise. For the function f, we observed the best performance for the median.

The final weight is the combination of W_{st} and W_{lrn},

$$W(\lambda_{ij}) = W_{st}(v_j, c_i) \cdot W_{lrn}(\lambda_{ij}). \tag{6}$$
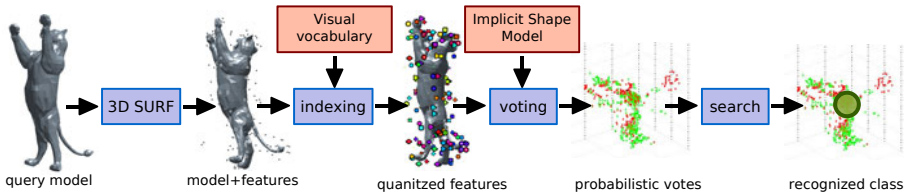
Fig. 6. Overview of our 3D ISM class recognition. On the query shape, 3D SURF features are detected, described and quantized into the visual vocabulary. Using the previously trained 3D Implicit Shape Model, each visual word then generates a set of votes for the position of the class center and the relative shape size. Finally, the recognized class is found at the location with maximum density of these votes.

3.3 Determining a Query Shape's Class

The class recognition decision for a given 3D query shape is determined by the set of 5D votes (shape center, size of the shape and class), weighted by the function W. However, we need a mechanism to cluster votes cast at nearby but distinct locations. Depending on the type of query shape, we use one of two approaches:

1. *Cube Searching (CS):* In the spirit of Leibe *et al.* [16], we discretize the 5D search space into bins; each vote contributes to all bins based on its Gaussian-weighted distance to them. The recognized class and shape center is given by the highest score. The principal advantage of this approach is that it does not require a clean query shape—noisy or partial query input is handled by explicitly searching for the optimal shape center as well as the class.
2. *Distance to Shape Center (DC):* Unlike image queries, where the shape's center within the image is usually unknown, it is quite easy to compute the centroid of a clean 3D shape, and use this as the shape center. Doing so can simplify class recognition and improve its robustness by reducing the search to the best class given this center. We do this by weighting each vote by a Gaussian of its distance to the query shape's center. Processing of such complete 3D shapes is a popular task in the 3D literature [11,10]. Obviously, the real object center coinciding with the shape center is not always valid and we cannot use it for partial shapes or for the recognition of 3D scenes (with additional clutter or noise).

4 Experiments and Applications

Our main target is to robustly classify 3D shapes. Having visually assessed the 3D SURF descriptors (§ 2) in Figs. (3,4), we evaluate it further for the difficult task of partial shape retrieval in § 4.2. Since the task is retrieval, the features are used in the BOF framework for this test. Supported by the good performance, we further use 3D SURF features in conjunction with the probabilistic Hough

voting method of § 3 (ISM) to demonstrate its power for class recognition and for assessing the sensitivity to missing data on standard datasets. Our proposed method outperforms the other approaches in these clean shape datasets. Finally, we tackle classification of 3D scenes reconstructed from real life images. Such scenes are challenging due to clutter, noise and holes. We show promising results on such data in § 4.4.

4.1 Datasets

All the datasets (Fig. 9) used in our evaluations consists of clean and segmented shapes and are defined at the outset.

(i) KUL dataset: simple dataset of 94 training shapes of 8 classes from the Internet and 22 query shapes.
(ii) Princeton dataset: challenging dataset of 1.8K shapes (half training, half testing), 7 classes taken from the Princeton Benchmark [24].
(iii) Tosca+Sumner dataset: dataset for retrieval/classification [25,26] of 474 shapes, 12 classes of which 66 random ones form a test set.
(iv) SHREC'09 datasets: 40 classes, 720 training and 20 partial query shapes from the Partial Shape Retrieval Contest [27] with complete ground-truth.

4.2 3D SURF Features for Shape Retrieval

We have presented a novel method for local features extraction and description for 3D shapes. We investigate now the performance of our approach to the state of the art descriptors.

As the task here is that of shape retrieval (as opposed to our classification based method from § 3), we use 3D SURF features in the large-scale image retrieval approach of Sivic and Zisserman [19] based on BOF. First, 3D SURF features of all shapes were quantized using the visual vocabulary as in § 3. Second, we compute the BOF vectors. Third, using the BOF, every shape model is represented as the normalized tf-idf vector [28] preferring the discriminative visual words. Finally, the similarity between shapes is measured as the L_1 distance between the normalized tf-idf vectors. L_1 measure was shown to perform better than the dot-product in image retrieval [19].

For the problem of partial shape retrieval 3D SURF is pitched against other descriptors in the SHREC'09 Contest [27] for the dataset (iv) in § 4.1. Fig. 7(a) presents our results together with results from the SHREC'09 Contest. Note that 3D SURF features outperform the rendered range-images -based SIFT descriptors [27], in similar BOF frameworks.

Fig. 7(b,c) shows the retrieval performance on two additional datasets. As the main result, we observed high sensitivity of all descriptors to to the dataset type, i.e. SI [15] outperforms all methods in Tosca dataset, while it gives the worst results on KUL dataset, but couldn't be evaluated on SHREC'09 due to computational constraints.
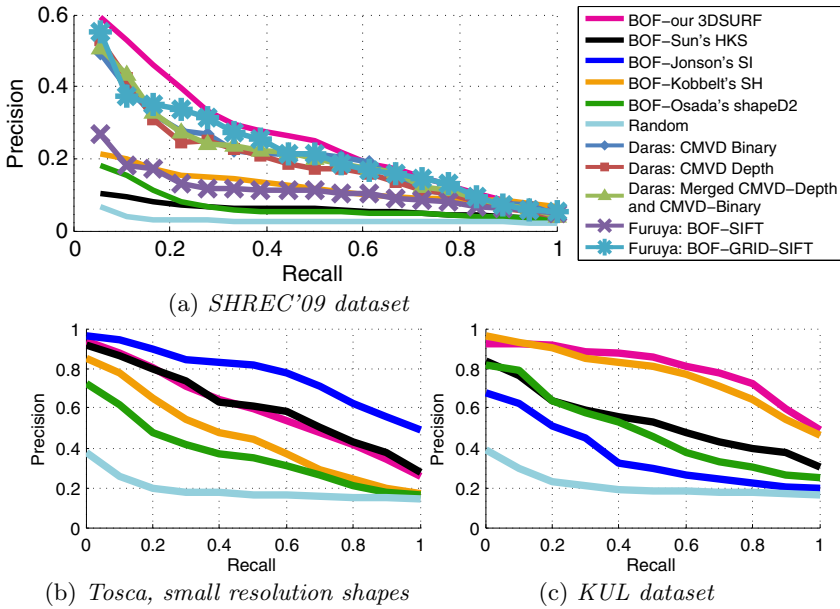
(a) *SHREC'09 dataset*

(b) *Tosca, small resolution shapes*   (c) *KUL dataset*

Fig. 7. Comparison of different detectors/descriptors using the video google [19] retrieval approach. The performance is measured as Precision-Recall curve. (a) SHREC'09 Partial Shape Retrieval Contest [27] provided results which were compared with our 3D SURF and other approaches. (b,c) Note that the performance highly depends on the shape's type as results very depend on dataset.
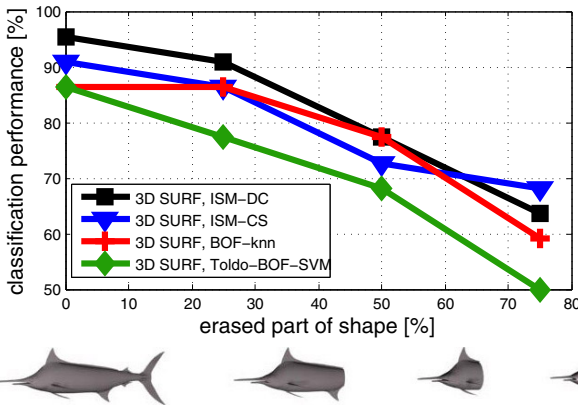

Fig. 8. Sensitivity of 3D classification to missing data. The classification performance is plotted as the shape is increasingly cropped. See the fish example on the bottom row. We found that our approach outperforms knn as well as Toldo's [11] SVM method.

We also observed (on shapes from 1.2K-65K faces and 670-33K vertices) that our method is faster than other local descriptors. In average, 3D SURF takes 20.66s, HKS [6] 111.42s and SI [15] more than 15mins. The experiment was performed on 4xQuad Core AMD Opteron, 1.25Ghz/core.

4.3   3D SURFs in the ISM Framework for 3D Classification

Here we apply our method (ISM, § 3) for shape classification in these variations:

(a) **ISM-CS:** with the cube-searching method from § 3.3 (1).
(b) **ISM-DC:** with the assumption that the shape's centre is known (see § 3.3 (2)).

The above versions of our method are compared against the following:

(i) **BOF-knn:** Encouraged by the good results of the 3D shape retrieval algorithm in § 4.2, we use this as one competitor. The test query shape is assigned to the most commonly occurring class of the best k-retrieved training shapes in a nearest-neighbor classification approach. Parameter k was learnt to optimize classification of train shapes. The shapes are represented by normalized tf-idf vectors and L_1 is used as metric.

(ii) **Toldo-BOF-SVM:** This is our implementation of Toldo *et al.* [11], where BOF vectors are computed on the training data $\mathcal{M}_T$. Then, the multi-class SVM classifier ([29]) is learned on the BOF vectors to predict the class label of the query shapes $\mathcal{M}_Q$. The kernel function is defined in terms of histogram intersection as in [11].

First, we investigate the sensitivity of classification methods with respect to the occlusions. Fig. 8 shows the performance of methods in the presence of occlusion on KUL dataset (§ 4.1 (i)). ISM-DC gives the best results for complete models and the performance of ISM-CS outperforms all methods with the more partial queries.

Table 1 summarizes all results on standard datasets of 3D shapes. Here, we measured the performance of classification methods on several datasets. Our approach using the Hough voting gave the average performance (see the last column in Table 1). The Princeton dataset (§ 4.1 (ii)) is the most challenging and although all methods gave similar results, we outperform the others. This dataset has very high variation amongst its 3D models *i.e.* the animal class contains widely varying models of 'ant' and 'fish'. For an SVM to learn a good classifier, we need a good non-linear kernel which has learnt such differences well. In such cases, non-parametric nearest-neighbor classifiers have a natural advantage.

The SHREC'09 dataset (§ 4.1 (iv)), previously used for the retrieval of partial queries, is now used for classification. ISM doesn't perform well as this method needs relatively large number of training examples [16,21] which is not satisfied in this case.

We conclude that our ISM based method beats k-nn and SVM in most cases.

4.4   3D Shape Classification of Reconstructed Real Life Scenes

As a final note, it is interesting to investigate the relative roles 2D and 3D object class detection could play in real-life. We carry out a small experiment to see whether 3D detection would really offer an added value.

Given many images taken in uncontrolled conditions around a real object, state-of-the-art methods such as the Arc3D web-service [30] can be used to

Princeton:

Tosca+Sumner:

SHREC'09:

Fig. 9. Samples of query shapes from the state-of-the-art datasets

Table 1. Table summarizes all results of classification on state-of-the-art datasets. Proposed approach beats k-nn and SVM in most cases.

method	Princeton			Tosca+Sumner			SHREC'09			avg. perf.
	# TP	# FP	perfor.	# TP	# FP	perfor.	# TP	# FP	perfor.	
ISM	**529**	**378**	**58.3%**	**56**	**1**	**98%**	8	14	40%	**65.4%**
BOF-knn	491	416	54.1%	**56**	**1**	**98%**	7	13	35%	**62.4%**
BOF-SVM	472	435	52.0%	41	16	72%	**12**	**8**	**60%**	**61.3%**

bike: 12 out of 15

plant: 0 out of 81

woman: 47 out of 100

cube: n/a

people: 18 out of 18
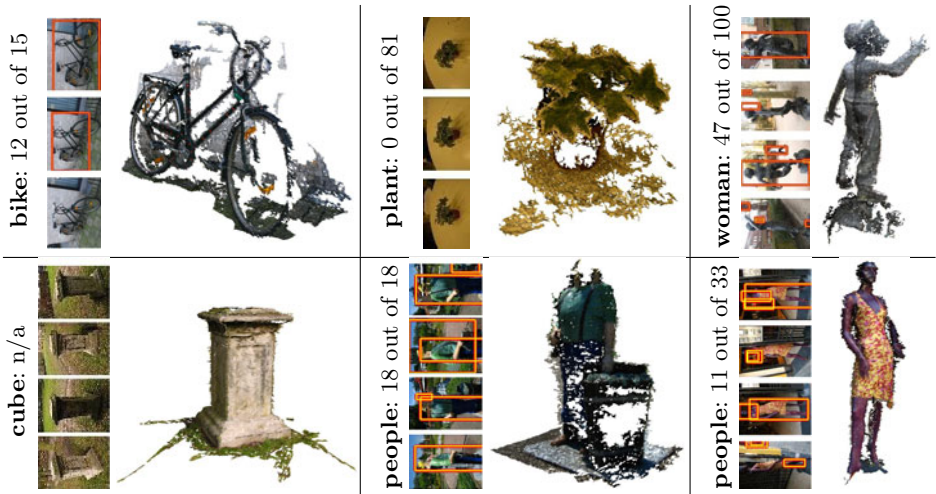
people: 11 out of 33

Fig. 10. 3D class recognition from the set of images. For each sample: correctly recognized class using 3D ISM, the number of correctly recognized objects in images using the method of Felzenszwalb *et al.* [31] (the best for PASCAL'08), samples of detection results are highlighted by squares, and the reconstructed shape by Arc3D [30].

extract a dense 3D model from the captured images. Such object models exhibit varying amounts of noise, holes and clutter from the surroundings, as can be seen from the examples (see Fig. 10). For each class on Fig. 10 we reuse the 3D ISM models trained on datasets of the SHREC'09 (for bike and plant classes),

Tosca+Sumner (for woman) and KUL (for cube and people). We also used 2D Felzenszwalb detectors [31] trained on data from the PASCAL'08 datasets for bikes, potted plants, and pedestrians. As shown in the Fig. 10, a small test was run, where 3D reconstructions were produced from images for an instance of each of the 6 objects. In each of these cases, the classification using 3D ISM was successful, while SVM based method of Toldo *et al.* [11] failed in all cases. As to the 2D detectors, the bike was found in 12 out of the 15 images, the potted plant in none of the 81 images, and the person in 47 out of the hundred. This would indicate that given a video images input, a single 3D detection into the images could be more effective than 2D detections in separate images. But issues concerning 2D vs. 3D detection need to be explored further.

5   Conclusion

In this paper, we introduced 3D SURF features in combination with the probabilistic Hough voting framework for the purpose of 3D shape class recognition. This work reaffirms the direction taken by recent research in 2D class detection, but thereby deviates rather strongly from traditional 3D approaches, which are often based on global features, and where only recently some first investigations into local features combined with bag-of-features classification were made.

We have demonstrated through experiments, first the power of the features (§ 4.2), followed by the combined power of the features and the classification framework (§ 4.3). This method outperforms existing methods and both aspects seem to play a role in that.

References

1. Kobbelt, L., Schrder, P., Kazhdan, M., Funkhouser, T., Rusinkiewicz, S.: Rotation invariant spherical harmonic representation of 3d shape descriptors (2003)
2. Saupe, D., Vranic, D.V.: 3d model retrieval with spherical harmonics and moments. In: Radig, B., Florczyk, S. (eds.) DAGM 2001. LNCS, vol. 2191, p. 392. Springer, Heidelberg (2001)
3. Osada, R., Funkhouser, T., Chazelle, B., Dobki, D.: Shape distributions. ACM Transactions on Graphics, 807–832 (2002)
4. Leymarie, F.F., Kimia, B.B.: The shock scaffold for representing 3d shape. In: Workshop on Visual Form (IWVF4) (2001)
5. Mian, A.S., Bennamoun, M., Owens, R.: Three-dimensional model-based object recognition and segmentation in cluttered scenes. IEEE PAMI 28 (2006)
6. Sun, J., Ovsjanikov, M., Guibas, L.: A concise and provably informative multi-scale signature based on heat diffusion. In: SGP, pp. 1383–1392 (2009)
7. Gelfand, N., Mitra, N.J., Guibas, L.J., Pottmann, H.: Robust global registration. In: Symposium on Geometry Processing, pp. 197–206 (2005)
8. Pottmann, H., Wallner, J., Huang, Q.X., Yang, Y.L.: Integral invariants for robust geometry processing. Comput. Aided Geom. Des. 26, 37–60 (2009)

9. Novatnack, J., Nishino, K.: Scale-dependent/invariant local 3d shape descriptors for fully automatic registration of multiple sets of range images. In: Forsyth, D., Torr, P., Zisserman, A. (eds.) ECCV 2008, Part III. LNCS, vol. 5304, pp. 440–453. Springer, Heidelberg (2008)
10. Ovsjanikov, M., Bronstein, A.M., Bronstein, M.M., Guibas, L.J.: Shapegoogle: a computer vision approach for invariant shape retrieval (2009)
11. Toldo, R., Castellani, U., Fusiello, A.: A bag of words approach for 3d object categorization. In: Gagalowicz, A., Philips, W. (eds.) MIRAGE 2009. LNCS, vol. 5496, pp. 116–127. Springer, Heidelberg (2009)
12. Golovinskiy, A., Kim, V.G., Funkhouser, T.: Shape-based recognition of 3d point clouds in urban environments. In: ICCV (2009)
13. Brostow, G.J., Shotton, J., Fauqueur, J., Cipolla, R.: Segmentation and recognition using structure from motion point clouds. In: Forsyth, D., Torr, P., Zisserman, A. (eds.) ECCV 2008, Part I. LNCS, vol. 5302, pp. 44–57. Springer, Heidelberg (2008)
14. Bay, H., Ess, A., Tuytelaars, T., Van Gool, L.: Speeded-up robust features (surf). Comput. Vis. Image Underst. 110, 346–359 (2008)
15. Johnson, A.E., Hebert, M.: Using spin images for efficient object recognition in cluttered 3d scenes. IEEE PAMI 21, 433–449 (1999)
16. Leibe, B., Leonardis, A., Schiele, B.: Robust object detection with interleaved categorization and segmentation. IJCV 77, 259–289 (2008)
17. Willems, G., Tuytelaars, T., Van Gool, L.: An efficient dense and scale-invariant spatio-temporal interest point detector. In: Forsyth, D., Torr, P., Zisserman, A. (eds.) ECCV 2008, Part II. LNCS, vol. 5303, pp. 650–663. Springer, Heidelberg (2008)
18. Muja, M., Lowe, D.: Fast approximate nearest neighbors with automatic algorithm configuration. In: VISAPP (2009)
19. Sivic, J., Zisserman, A.: Video Google: A text retrieval approach to object matching in videos. In: ICCV (2003)
20. Jégou, H., Douze, M., Schmid, C.: Improving bag-of-features for large scale image search. IJCV (2010) (to appear)
21. Lehmann, A., Leibe, B., Gool, L.V.: Feature-centric efficient subwindow search. In: ICCV (2009)
22. Philbin, J., Chum, O., Isard, M., Sivic, J., Zisserman, A.: Lost in quantization: Improving particular object retrieval in large scale image databases. In: CVPR (2008)
23. Maji, S., Malik, J.: Object detection using a max-margin hough transform. In: CVPR, pp. 1038–1045 (2009)
24. Shilane, P., Min, P., Kazhdan, M., Funkhouser, T.: The princeton shape benchmark. In: Shape Modeling International (2004)
25. Bronstein, A., Bronstein, M., Kimmel, R.: Numerical Geometry of Non-Rigid Shapes. Springer Publishing Company, Incorporated, Heidelberg (2008)
26. Sumner, R.W., Popovic, J.: Deformation transfer for triangle meshes. ACM Trans. Graph. 23, 399–405 (2004)
27. Dutagaci, H., Godil, A., Axenopoulos, A., Daras, P., Furuya, T., Ohbuchi, R.R.: Shrec 2009 - shape retrieval contest of partial 3d models (2009)
28. Salton, G., Buckley, C.: Term-weighting approaches in automatic text retrieval. Inf. Process. Manage. 24, 513–523 (1988)
29. Chang, C.C., Lin, C.J.: LIBSVM: a library for support vector machines (2001) Software available at http://www.csie.ntu.edu.tw/~cjlin/libsvm
30. Vergauwen, M., Gool, L.V.: Web-based 3d reconstruction service. Mach. Vision Appl. 17, 411–426 (2006)
31. Felzenszwalb, P.F., Girshick, R.B., McAllester, D., Ramanan, D.: Object detection with discriminatively trained part based models. IEEE PAMI 99 (2009)